The 8th European Congress on Computational Methods in Applied Sciences and Engineering
ECCOMAS Congress 2022
5-–9 June 2022, Oslo, Norway

INCORPORATING EFFECTIVE TRANSMISSION CONDITIONS BETWEEN FLUID AND SOLID DOMAINS IN TRANSIENT WAVE PROPAGATION PROBLEMS USING THE MORTAR ELEMENT METHOD

Alexandre Imperiale[1]

[1] Université Paris-Saclay, CEA, List, F-91120, Palaiseau, France, alexandre.imperiale@cea.fr

Key words: Transient Wave Propagation, Acoustic – Elastic waves interactions, Domain Decomposition Methods, Time Discretization, Ultrasonic Testing Modeling.

Abstract. We derive an efficient numerical scheme for transient wave propagation in configurations where a fluid domain and a solid domain are separated by a thin coating material. These type of configurations are numerically challenging for multiple factors: managing fluid – solid coupling, enabling non-conform space discretizations, and rendering robust time discrete algorithm *w.r.t* the thin layer thickness. By combining the mortar element method with effective transmission conditions we are able to address these challenges. We illustrate our approach by proposing relevant 2D numerical illustrations inspired from simple ultrasonic testing experiments.

1 INTRODUCTION

In the present communication, we consider the problem of efficient numerical modeling of high-frequency transient wave propagation in a configuration where a solid material is surrounded by a fluid, and at the fluid – solid interface a thin layer of material is present. This configuration typically occurs when representing Ultrasonic Testing (UT) of immersed coated specimens. The computational challenges associated to this type of configurations are threefold:

(1) The thickness of the coating material, denoted by η in the following, is significantly smaller than the wavelength of interest, thus degrading the efficiency of standard approaches with explicit time scheme, as they suffer from a stability condition on the time step in $O(\eta)$.

(2) In UT applications, the wavelength in the fluid are usually smaller than in the solid (due to lower wave velocities). Hence traditional conform approaches will impose an over-refined mesh in the solid domain, leading to a potentially significant cost overhead.

(3) As any fluid – structure interaction problem, one has to operate a specific treatment in order to incorporate the normal stress and normal velocity continuity conditions within their numerical scheme.

Various tools and techniques can be found in the literature to overcome some of these computational bottlenecks. For instance, authors in [1] use an implicit scheme (only) in the thin layer. Their approach alleviates the dependency of the time step *w.r.t.* the layer thickness.

It is based on the mortar element method [2] allowing for non-conform coupling between the domains. However it is done at the price of solving at each iteration a linear system of size proportionate to the number of degrees of freedom in the layer and should require some adjustment to incorporate fluid – solid transmission conditions. In [3] a local time stepping method is proposed which effectively reduces the influence of refined or complex regions of the mesh onto the stability condition of the explicit time scheme. Essentially, this is performed by adding subiterations between coarse time steps. Their approach imposes the use of discontinuous Galerkin methods [4] in order to address non-conform meshes, and cannot support as-is coupling between fluid and solid propagators. Other approaches rely on a simplification of the wave propagator in the coating layer based upon asymptotic developments – the asymptotic parameter being proportionate to the thickness η. A typical example in the literature is [5]. More recently authors in [6] derived Effective Transmission Conditions (ETC) between two solid domains surrounding the layer while insuring convergence to the exact solution as the thickness tends to zero. Their effective numerical procedure leads to a time step independent of the layer thickness, however supporting acoustic – elastic waves coupling with non-conforming meshes is not addressed in their approach.

Inspired from this seminal body of work, our approach combine the use of ETC – as in [5] – with an adequate form of the mortar element method – as in [1]. It is in essence the extension of [7] to configurations with fluid and solid propagators. The mortar unknowns are treated with an implicit time-scheme, from which we can expect the stability condition of the complete numerical procedure to be independent of the layer thickness or effective parameters. This method supports (by construction) non-conform meshes, and we are able to adapt it to support fluid – solid coupling. Combining these elements we are able to address the various computational challenges associated to the configurations of interest.

The outline of our paper is as follows. In Section 2 we detail the modeling setting used to represent UT experiments of an immersed and coated solid material. In Section 3 we present the numerical procedure leading to a fully discrete scheme. This procedure combine spectral finite elements [9] for the space discretization and second order schemes [8] for the time discretization. We illustrate our approach in Section 4 with some relevant numerical results, and provide some conclusion and perspectives in the last Section.

2 WAVE PROPAGATION THROUGH AN IMMERSED AND COATED SOLID

2.1 Geometrical considerations

Let $N = 2$ or $N = 3$ denotes the space dimension. As depicted in Figure 1, we consider the open domain $\Omega_{\rm s} \subset \mathbb{R}^N$ occupied by a solid material subject to an UT experiment. This solid material is partially adjacent to a fluid (typically water) occupying the fluid domain $\Omega_{\rm f}$. Between the solid and fluid domains, we consider a thin coating material occupying the volume Ω^η, where η represents an upper bound of the (local) thickness of the coating domain. As a basic assumption of the following developments, we assume that η is significantly smaller that the wavelengths of interest, hence justifying the label of "coating" domain.

Additionally, we consider an extruded structure of Ω^η that we detail in this subsection in a 2D context for simplicity – the extension for $N = 3$ being conceptually straightforward. Let Γ represents the "middle" line of the domain characterized by its parametric coordinate

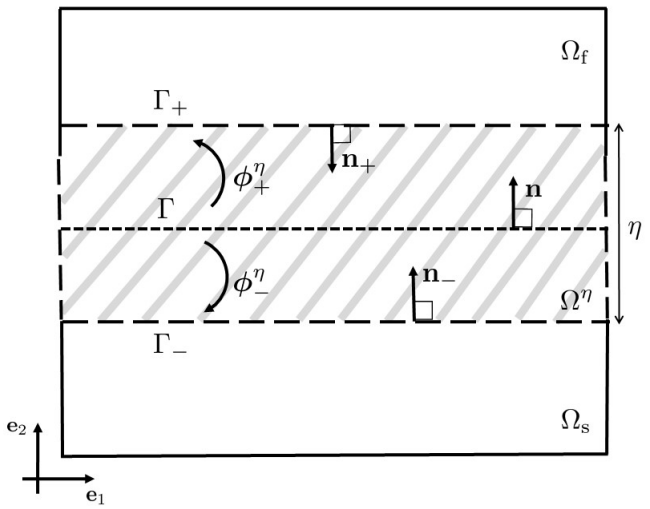

Figure 1: Representation of the type of geometrical configuration of interest for $N = 2$. The hatched area, above the solid domain Ω_s and below the fluid domain Ω_f, represents the coating layer Ω^η.

transformation $\boldsymbol{\psi} : [0;1] \mapsto \mathbf{x} \in \Gamma$, assumed to be a $\mathcal{C}^1$ – diffeomorphism. Let $\Gamma_\pm$ be the "upper" and "lower" boundary lines of the domain. They are obtained from the middle line through the transformations $\boldsymbol{\phi}_\pm^\eta : \mathbf{x} \mapsto \mathbf{x}' \in \Gamma_\pm$, *i.e.*

$$\Gamma_\pm = \Big\{ \mathbf{x}' \;\Big|\; \mathbf{x}' = \boldsymbol{\phi}_\pm^\eta\big(\boldsymbol{\psi}(u)\big), \quad \forall u \in [0;1] \Big\}.$$

These transformations depend on the upper bound of the thickness η and are also assumed to be $\mathcal{C}^1$ – diffeomorphisms. The remaining "left" and "right" boundary lines of the domain denoted by Γ_0 and Γ_1 are segments defined as

$$\forall \beta \in \{0,1\}, \quad \Gamma_\beta = \Big\{ \mathbf{x}' \;\Big|\; \mathbf{x}' = v\boldsymbol{\phi}_+^\eta\big(\boldsymbol{\psi}(\beta)\big) + (1-v)\boldsymbol{\phi}_-^\eta\big(\boldsymbol{\psi}(\beta)\big), \quad \forall v \in [0;1] \Big\},$$

and we define the domain Ω^η as the open set with boundary $\partial\Omega^\eta = \Gamma_+ \cup \Gamma_- \cup \Gamma_0 \cup \Gamma_1$ – see Figure 1 for a representation of such configurations.

2.2 Elastic and acoustic linear wave propagation models

Within the solid domain, we consider $\mathbf{u}$ the space and time dependent material displacement generated by the high-frequency and low amplitude waves during their course. Internal mechanical stresses $\boldsymbol{\sigma}$ are associated to this displacement. As standard in ultrasonic wave propagation modeling, we assume a fully linear constitutive law, and in the particular case of this communication we consider – without loss of generality – an isotropic material. In this context we recover Hooke's law

$$\boldsymbol{\sigma}(\mathbf{u}) = \lambda \mathrm{tr}(\boldsymbol{\varepsilon}(\mathbf{u}))\mathbf{I} + 2\mu\boldsymbol{\varepsilon}(\mathbf{u}), \quad \boldsymbol{\varepsilon}(\mathbf{u}) = \tfrac{1}{2}\big(\boldsymbol{\nabla}\mathbf{u} + \boldsymbol{\nabla}\mathbf{u}^\intercal\big),$$

where $\boldsymbol{\varepsilon}(\mathbf{u})$ is the linearized Green – Lagrange tensor associated to the displacement $\mathbf{u}$, $\mathrm{tr}(\cdot)$ is the trace of a second order tensor, $\mathbf{I}$ is the identity second order tensor, and $\{\lambda, \mu\}$ are the Lamé's coefficients. In addition to this constitutive law, we recall the standard linear elasto-dynamic equation

$$\rho_{\mathrm{s}} \partial_{tt}^2 \mathbf{u} - \boldsymbol{\nabla} \cdot \boldsymbol{\sigma}(\mathbf{u}) = 0, \quad \text{in} \quad \Omega_{\mathrm{s}}, \tag{1}$$

where $\boldsymbol{\nabla}\cdot$ is the divergence operator applied to second order tensors, and ρ_{s} is the mass density of the material.

Within the fluid domain, we consider $\mathbf{v}$ the velocity field and p the pressure field associated to the acoustic wave propagation. They are linked through the standard wave equations

$$\frac{1}{\rho_{\mathrm{f}} c^2} \partial_t p + \nabla \cdot \mathbf{v} + f = 0, \quad \rho_{\mathrm{f}} \partial_t \mathbf{v} + \nabla p = 0, \quad \text{in} \quad \Omega_{\mathrm{f}}, \tag{2}$$

where f is a time and space dependent source term representing some known acoustic emitter, $\nabla\cdot$ is the divergence operator applied to vector fields, c is the speed of waves in the fluid domain, and ρ_{f} is the mass density of the fluid. Defining ϕ the acoustic velocity potential such that

$$\mathbf{v} = \frac{1}{\rho_{\mathrm{f}}} \boldsymbol{\nabla} \phi, \quad p = -\partial_t \phi, \tag{3}$$

where the second relation is obtained using (2), we recover the traditional second order wave equation

$$\frac{1}{\rho_{\mathrm{f}} c^2} \partial_{tt}^2 \phi - \frac{1}{\rho_{\mathrm{f}}} \Delta \phi = f, \quad \text{in} \quad \Omega_{\mathrm{f}}. \tag{4}$$

2.3 Effective transmission conditions to represent the coating material

To represent the propagation within the coating material, we resort to effective transmission conditions (ETC) as in [5] that we adapt to fluid – solid coupling. To simplify the presentation, we will use extensively the following notation

$$\forall d \in \{1, N\}, \quad \forall \mathbf{f} \in [L^2(\Gamma_\pm)]^d, \quad \mathbf{f}_\pm = \mathbf{f} \circ \boldsymbol{\phi}_\pm^\eta \in [L^2(\Gamma)]^d.$$

In particular, we define the mechanical fluxes associated to the fluid and solid fluxes as

$$\boldsymbol{\tau}_+ = -p_+ \, \mathbf{n}, \quad \boldsymbol{\tau}_- = \boldsymbol{\sigma}_- \cdot \mathbf{n}, \quad \text{on} \quad \Gamma.$$

The mean value and jump of the fluxes are denoted by

$$\langle \boldsymbol{\tau} \rangle = \frac{\boldsymbol{\tau}_+ + \boldsymbol{\tau}_-}{2}, \quad [\boldsymbol{\tau}] = \boldsymbol{\tau}_+ - \boldsymbol{\tau}_-.$$

In the same manner, we define the mean value and jump of velocities on Γ as

$$\langle \mathbf{v} \rangle = \frac{\mathbf{v}_+ + \partial_t \mathbf{u}_-}{2}, \quad [\mathbf{v}] = \mathbf{v}_+ - \partial_t \mathbf{u}_-.$$

Without the presence of the coating layer, implying in particular that $\boldsymbol{\phi}_\pm^\eta = \mathbf{I}$, satisfying the standard fluid – solid transmission conditions implies

$$[\mathbf{v}] \cdot \mathbf{n} = 0, \quad [\boldsymbol{\tau}] = 0, \quad \text{on} \quad \Gamma,$$

which is essentially the continuity of the normal velocities and the mechanical fluxes. Note that, because of the form of the fluid flux, this is equivalent to satisfying

$$[\mathbf{v}]\cdot\mathbf{n}=0,\quad [\boldsymbol{\tau}]\cdot\mathbf{n}=0,\quad \boldsymbol{\tau}_-\cdot\mathbf{n}^\perp=0,\quad \text{on}\quad \Gamma,$$

where $\mathbf{n}^\perp$ is any tangent vector of Γ. The underlying idea behind ETC, as in [5, 10], is to perturb the two jump relations with spring – mass terms using the mean fluxes and velocities, namely

$$[\mathbf{v}]\cdot\mathbf{n}=\eta\mathrm{s}\,\partial_t\langle\boldsymbol{\tau}\rangle\cdot\mathbf{n},\quad [\boldsymbol{\tau}]\cdot\mathbf{n}=\eta\mathrm{m}\,\partial_t\langle\mathbf{v}\rangle\cdot\mathbf{n},\quad \text{on}\quad \Gamma. \tag{5}$$

Here s and m are the effective normal compliance and mass density of the coating layer. As an illustrative example, in the case of an isotropic coating material in 2D admitting $\{\lambda',\mu'\}$ as Lamé's parameters and ρ' as mass density, a typical choice of effective parameters is

$$\mathrm{s}=\frac{1}{\lambda'+2\mu'},\quad \mathrm{m}=\rho'. \tag{6}$$

In the following, without loss of generality and to simplify the presentation, we will assume that both the thickness η and the effective parameters $\{\mathrm{s},\mathrm{m}\}$ are constant *w.r.t.* space variables.

2.4 Mortar elements and coupled weak formulation

Incorporating such transmission conditions (especially in a potentially non-conform context) is not self-evident. To address this challenge we resort to the mortar element method [2]. It is originally a domain decomposition approach enabling coupling of non-conforming space discretizations. Recently [7] it has been used to incorporate ETC between two solids and we extend this approach to fluid – solid coupling. To start with, we define the following unknowns

$$\partial_t\lambda_\mathrm{f}=\mathbf{v}_+\cdot\mathbf{n},\quad \partial_t\lambda_\mathrm{s}=\boldsymbol{\tau}_-\cdot\mathbf{n}, \tag{7}$$

which are, for any fixed time value, elements of $L^2(\Gamma)$. Using this definition and the jump relations (5) we have

$$\partial_t\lambda_\mathrm{f}-\partial_t\mathbf{u}_-\cdot\mathbf{n}=\eta\mathrm{s}\frac{\partial^2_{tt}\phi_+ +\partial^2_{tt}\lambda_\mathrm{s}}{2},\quad \partial_t\phi_+-\partial_t\lambda_\mathrm{s}=\eta\mathrm{m}\frac{\partial^2_{tt}\lambda_\mathrm{f}+\partial^2_{tt}\mathbf{u}_-\cdot\mathbf{n}}{2},$$

which can be integrated over time to reduce the order of time derivation. Satisfying these conditions weakly, and combining with the weak form of formulations (1) and (4) yields the following fully coupled weak formulation:

Find $\{\phi(t),\mathbf{u}(t),\lambda_\mathrm{f}(t),\lambda_\mathrm{s}(t)\}\in H^1(\Omega_\mathrm{f})\times[H^1(\Omega_\mathrm{s})]^N\times L^2(\Gamma)\times L^2(\Gamma)$ such that

$$\left|\begin{array}{l}
\dfrac{\mathrm{d}^2}{\mathrm{d}t^2}\displaystyle\int_{\Omega_\mathrm{f}}\tfrac{1}{\rho_\mathrm{f}c^2}\phi\,\phi^\star\,\mathrm{d}\Omega+\int_{\Omega_\mathrm{f}}\tfrac{1}{\rho_\mathrm{f}}\boldsymbol{\nabla}\phi\cdot\boldsymbol{\nabla}\phi^\star\,\mathrm{d}\Omega+\dfrac{\mathrm{d}}{\mathrm{d}t}\displaystyle\int_\Gamma\lambda_\mathrm{f}\,\phi^\star_+\,\mathrm{d}\Gamma=\int_{\Omega_\mathrm{f}}f\,\phi^\star\,\mathrm{d}\Omega,\\
\dfrac{\mathrm{d}^2}{\mathrm{d}t^2}\displaystyle\int_{\Omega_\mathrm{s}}\rho_\mathrm{s}\mathbf{u}\cdot\mathbf{u}^\star\,\mathrm{d}\Omega+\int_{\Omega_\mathrm{s}}\boldsymbol{\sigma}(\mathbf{u}):\boldsymbol{\varepsilon}(\mathbf{u}^\star)\,\mathrm{d}\Omega-\dfrac{\mathrm{d}}{\mathrm{d}t}\displaystyle\int_\Gamma\lambda_\mathrm{s}\,\mathbf{u}^\star_-\cdot\mathbf{n}\,\mathrm{d}\Gamma=0,\\
\dfrac{\mathrm{d}}{\mathrm{d}t}\displaystyle\int_\Gamma\eta\mathrm{m}\Big(\frac{\lambda_\mathrm{f}+\mathbf{u}_-\cdot\mathbf{n}}{2}\Big)\lambda^\star_\mathrm{f}\,\mathrm{d}\Gamma=\int_\Gamma(\phi_+-\lambda_\mathrm{s})\lambda^\star_\mathrm{f}\,\mathrm{d}\Gamma,\\
\dfrac{\mathrm{d}}{\mathrm{d}t}\displaystyle\int_\Gamma\eta\mathrm{s}\Big(\frac{\phi_++\lambda_\mathrm{s}}{2}\Big)\lambda^\star_\mathrm{s}\,\mathrm{d}\Gamma=\int_\Gamma(\lambda_\mathrm{f}-\mathbf{u}_-\cdot\mathbf{n})\lambda^\star_\mathrm{s}\,\mathrm{d}\Gamma,
\end{array}\right. \tag{8}$$

for any set of test functions $\{\phi^\star,\mathbf{u}^\star,\lambda^\star_\mathrm{f},\lambda^\star_\mathrm{s}\}\in H^1(\Omega_\mathrm{f})\times[H^1(\Omega_\mathrm{s})]^N\times L^2(\Gamma)\times L^2(\Gamma)$.

3 FULLY DISCRETE SCHEME

3.1 Space discretization using spectral finite elements

We discretize in space the weak formulation (8) using spectral finite elements [9]. In its original form, it is a H^1 – conform, high order finite element method, based on quadrangular or hexahedral meshes, with the Gauss – Lobatto distribution of nodes in the reference element. Let us denote by $\mathcal{T}_h(\overline{\Omega}_\mathrm{f})$ and $\mathcal{T}_H(\overline{\Omega}_\mathrm{s})$ conform meshes of the fluid and solid domains with characteristic mesh sizes h and H. In most cases, the gap between wave speeds in the two domains may require two different mesh sizes to obtain better performances. Therefore, in the following we assume that $h \leq H$, potentially entailing non-conformities at the coupling interface. For each element K in a mesh, we denote by $\mathbf{F}_K$ the associated transformation of the reference quadrangle or hexahedron $\widehat{K}$. On the reference element, we consider $\mathcal{Q}^\alpha(\widehat{K})$ the space of polynomials of maximal order $\alpha \in \mathbb{N}$. Let p and q be two given natural integers, we define the following finite element approximation spaces

$$\left|\begin{array}{ll} V_h &= \Big\{ v_h \in \mathcal{C}^0(\overline{\Omega}_\mathrm{f}) \;\Big|\; \forall K \in \mathcal{T}_h(\overline{\Omega}_\mathrm{f}),\ \exists!\, \widehat{v} \in \mathcal{Q}^p(\widehat{K}),\ v_h|_K = \widehat{v} \circ \mathbf{F}_K^{-1} \Big\} \subset H^1(\Omega_\mathrm{f}), \\ W_H &= \Big\{ w_H \in \mathcal{C}^0(\overline{\Omega}_\mathrm{s}) \;\Big|\; \forall K \in \mathcal{T}_H(\overline{\Omega}_\mathrm{s}),\ \exists!\, \widehat{w} \in \mathcal{Q}^q(\widehat{K}),\ w_H|_K = \widehat{w} \circ \mathbf{F}_K^{-1} \Big\} \subset H^1(\Omega_\mathrm{s}), \end{array}\right.$$

and the vectorial counterpart $\mathbf{W}_H = [W_H]^N \subset [H^1(\Omega_\mathrm{s})]^N$. Let N_f and N_s be the dimension of the approximation spaces V_h and $\mathbf{W}_H$ respectively, we consider

$$V_h = \mathrm{span}\,\{\varphi_I\}_{I=1}^{N_\mathrm{f}}, \quad W_H = \mathrm{span}\,\{\psi_I\}_{I=1}^{N_\mathrm{s}/N}, \quad \mathbf{W}_H = \mathrm{span}\,\{\boldsymbol{\psi}_I\}_{I=1}^{N_\mathrm{s}},$$

the associated Lagrange basis functions. Using these notations, we introduce the mass and stiffness matrices

$$\left|\begin{array}{ll} \mathbb{M}_\mathrm{f} = \Big(\displaystyle\int_{\Omega_\mathrm{f}} \tfrac{1}{\rho_\mathrm{f} c^2}\, \varphi_I\, \varphi_J \,\mathrm{d}\Omega \Big)_{I,J=1}^{N_\mathrm{f}} & , \quad \mathbb{M}_\mathrm{s} = \Big(\displaystyle\int_{\Omega_\mathrm{s}} \rho_\mathrm{s}\, \boldsymbol{\psi}_I \cdot \boldsymbol{\psi}_J \,\mathrm{d}\Omega \Big)_{I,J=1}^{N_\mathrm{s}}, \\ \mathbb{K}_\mathrm{f} = \Big(\displaystyle\int_{\Omega_\mathrm{f}} \tfrac{1}{\rho_\mathrm{f}}\, \boldsymbol{\nabla}\varphi_I \cdot \boldsymbol{\nabla}\varphi_J \,\mathrm{d}\Omega \Big)_{I,J=1}^{N_\mathrm{f}}, & \quad \mathbb{K}_\mathrm{s} = \Big(\displaystyle\int_{\Omega_\mathrm{s}} \boldsymbol{\sigma}(\boldsymbol{\psi}_I) : \boldsymbol{\varepsilon}(\boldsymbol{\psi}_J) \,\mathrm{d}\Omega \Big)_{I,J=1}^{N_\mathrm{s}}. \end{array}\right.$$

For the mortar unknowns, we consider the approximation space built from the trace of the scalar volume space W_H. More precisely, we define

$$X_H = \mathrm{span}\,\{\xi_\ell\}_{\ell=1}^{N_\Gamma} \subset L^2(\Gamma), \quad \forall \ell = 1, \cdots, N_\Gamma, \quad \exists!\, I \in \{1, \cdots, {}^{N_\mathrm{s}}/_N\}, \quad \xi_\ell = \psi_I|_{\Gamma_-} \circ \phi_-^\eta,$$

and N_Γ the number of nodes on Γ_-. With these basis functions, we define the coupling matrices (from mortar to volume unknowns) and the surface mass matrix

$$\mathbb{C}_\mathrm{f} = \Big(\int_\Gamma \varphi_{I+}\, \xi_\ell \,\mathrm{d}\Gamma \Big)_{I,\ell=1}^{N_\mathrm{f},N_\Gamma}, \quad \mathbb{C}_\mathrm{s} = \Big(\int_\Gamma \boldsymbol{\psi}_{I-} \cdot \mathbf{n}\, \xi_\ell \,\mathrm{d}\Gamma \Big)_{I,\ell=1}^{N_\mathrm{s},N_\Gamma}, \quad \mathbb{M}_\Gamma = \Big(\int_\Gamma \xi_\ell\, \xi_m \mathrm{d}\Gamma \Big)_{\ell,m=1}^{N_\Gamma}.$$

3.2 Time discretization and stability condition

Let us consider $\Delta t > 0$ a given time step – satisfying a specific stability condition discussed later on – and $n \in \mathbb{N}$ any step index. We consider $\overrightarrow{\phi}^n \in \mathbb{R}^{N_\mathrm{f}}$ the vector of components of the

discrete velocity potential in the basis of V_h at time $t^n = n\Delta t$. In the same manner we define $\overrightarrow{u}^n \in \mathbb{R}^{N_\mathrm{s}}$, $\overrightarrow{\lambda}^n_\mathrm{f} \in \mathbb{R}^{N_\Gamma}$ and $\overrightarrow{\lambda}^n_\mathrm{s} \in \mathbb{R}^{N_\Gamma}$ the vector of degrees of freedom in the basis of the relevant approximation space. With these notations, for the time discretization, we apply an explicit second order time-scheme centered at t^n for the volume propagators, and a second order time-scheme centered at $t^{n+1/2}$ for the transmission conditions, namely

$$\left|\begin{array}{l}
\frac{1}{\Delta t^2}\mathbb{M}_\mathrm{f}\big(\overrightarrow{\phi}^{n+1} - 2\overrightarrow{\phi}^{n} + \overrightarrow{\phi}^{n-1}\big) + \mathbb{K}_\mathrm{f}\overrightarrow{\phi}^{n} + \frac{1}{2\Delta t}\mathbb{C}_\mathrm{f}\big(\overrightarrow{\lambda}^{n+1}_\mathrm{f} - \overrightarrow{\lambda}^{n-1}_\mathrm{f}\big) = \overrightarrow{f},\\
\frac{1}{\Delta t^2}\mathbb{M}_\mathrm{s}\big(\overrightarrow{u}^{n+1} - 2\overrightarrow{u}^{n} + \overrightarrow{u}^{n-1}\big) + \mathbb{K}_\mathrm{s}\overrightarrow{u}^{n} - \frac{1}{2\Delta t}\mathbb{C}_\mathrm{s}\big(\overrightarrow{\lambda}^{n+1}_\mathrm{s} - \overrightarrow{\lambda}^{n-1}_\mathrm{s}\big) = 0,\\
\frac{\eta_\mathrm{m}}{2\Delta t}\mathbb{M}_\Gamma\big(\overrightarrow{\lambda}^{n+1}_\mathrm{f} - \overrightarrow{\lambda}^{n}_\mathrm{f}\big) + \frac{\eta_\mathrm{m}}{2\Delta t}\mathbb{C}_\mathrm{s}^\intercal\big(\overrightarrow{u}^{n+1} - \overrightarrow{u}^{n}\big) = \frac{1}{2}\mathbb{C}_\mathrm{f}^\intercal\big(\overrightarrow{\phi}^{n+1} + \overrightarrow{\phi}^{n}\big) - \frac{1}{2}\mathbb{M}_\Gamma\big(\overrightarrow{\lambda}^{n+1}_\mathrm{s} + \overrightarrow{\lambda}^{n}_\mathrm{s}\big),\\
\frac{\eta_\mathrm{s}}{2\Delta t}\mathbb{C}_\mathrm{f}^\intercal\big(\overrightarrow{\phi}^{n+1} - \overrightarrow{\phi}^{n}\big) + \frac{\eta_\mathrm{s}}{2\Delta t}\mathbb{M}_\Gamma\big(\overrightarrow{\lambda}^{n+1}_\mathrm{s} - \overrightarrow{\lambda}^{n}_\mathrm{s}\big) = \frac{1}{2}\mathbb{M}_\Gamma\big(\overrightarrow{\lambda}^{n+1}_\mathrm{f} + \overrightarrow{\lambda}^{n}_\mathrm{f}\big) - \frac{1}{2}\mathbb{C}_\mathrm{s}^\intercal\big(\overrightarrow{u}^{n+1} + \overrightarrow{u}^{n}\big).
\end{array}\right. \tag{9}$$

In the first line of (9), the values of the right-hand are simply given by the L^2 – inner product of the source function f with the basis functions of V_h.

Without carrying a complete analysis of the stability for (9), one can expect – since the dynamics satisfied by the mortar unknowns is discretized by an implicit scheme – to be able to derive the following stability condition

$$\Delta t \leq \min\left\{\frac{2}{\sqrt{r(\mathbb{M}_\mathrm{f}^{-1}\mathbb{K}_\mathrm{f})}}, \frac{2}{\sqrt{r(\mathbb{M}_\mathrm{s}^{-1}\mathbb{K}_\mathrm{s})}}\right\}, \tag{10}$$

where $r(\cdot)$ is the spectral radius of a matrix. Note that the two terms in the right hand side of the previous inequality are the stability conditions of the fully discrete fluid and solid propagators taken independently. In other words, if this condition would be sufficient to insure stability, it would mean that the time step is independent on both the coating layer thickness and the corresponding effective parameters.

4 NUMERICAL ILLUSTRATIONS

To illustrate the efficiency of our approach we consider a simple 2D case, where the fluid domain is composed of water and the solid domain is composed of a steel material, *i.e.*

$$\rho_\mathrm{f} = 1.0\,\mathrm{g}\cdot\mathrm{cm}^{-3},\ c = 1.5\,\mathrm{mm}\cdot\mu\mathrm{s}^{-1},\ \rho_\mathrm{s} = 8.0\,\mathrm{g}\cdot\mathrm{cm}^{-3},\ \lambda = 144\,\mathrm{GPa},\ \mu = 72\,\mathrm{GPa}.$$

The source term is a line source in the fluid with a central frequency of 1.0 MHz. The size of the domains are chosen to be proportionate to the pressure wavelengths, in particular the fluid domain is the square $25\lambda^\mathrm{f}_P \times 25\lambda^\mathrm{f}_P$, while the solid domain is the rectangle $25\lambda^\mathrm{f}_P \times 25\lambda^\mathrm{s}_P$. The thickness of the coating layer is set to be $\eta = \lambda^\mathrm{f}_P/10$ and the material of the layer is twice as stiff as the solid domain, *i.e.*

$$\rho' = \rho_\mathrm{s},\ \lambda' = 2\lambda,\ \mu' = 2\mu,$$

from which we can derive the effective transmission coefficients using (6). Concerning the discretization parameter we use spectral elements of order five with three elements per λ^f_P in the fluid domain. For the solid domain we consider both cases of conform discretization (where we impose the same discretization as the fluid domain) and non-conform discretization where

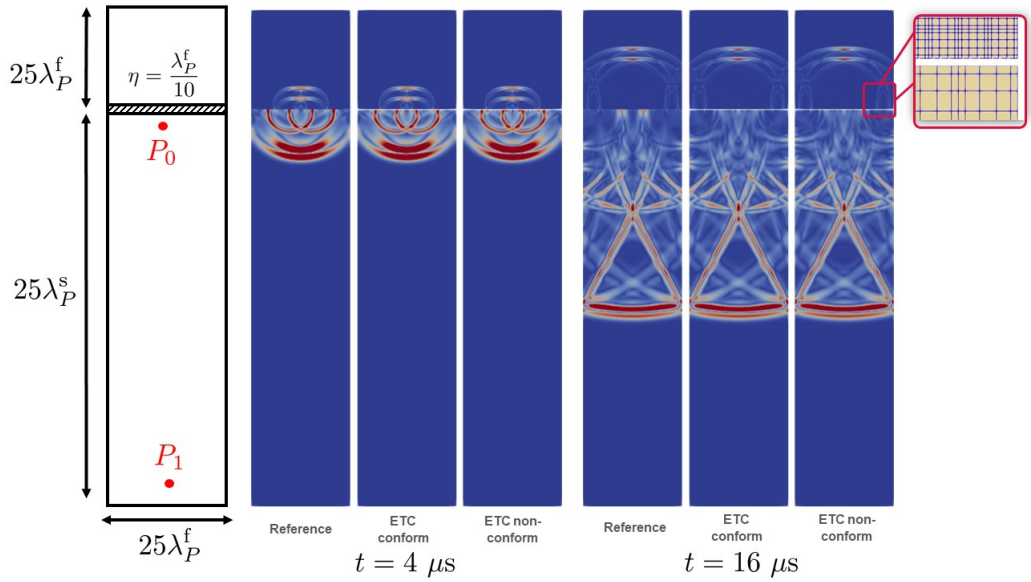

Figure 2: Illustration and snapshots of the solutions obtained by three different approaches: (i) meshed coating layer with conform interface (*i.e.* reference); (ii) ETC with conform interface; (iii) ETC with non-conform interface. Red dots represent the position of the observation points.

the order is still five but we set three elements per λ_P^{s}. We carry out numerical simulations by computing the upper bound on the time step provided in (10).

In Figure 2 we represent this configuration in addition with two snapshots where we compare: the reference simulation with conform interface and a meshed coating layer, a simulation using ETC with a conform interface and finally a simulation using ETC with a non-conform interface. In these snapshots we can see a very good agreement when comparing reflected pressure wave in the fluid and bulk waves in the solid (both pressure and transverse waves). We observe some discrepancies for the surface waves. These discrepancies appear even in the conform case, implying that the ETC cannot adequately capture these contributions.

To better validate the proposed numerical scheme we propose in Figure 3 to extract over time the solution at two observation points. As depicted in Figure 2, we position a first point near the interface and a second point far from the interface, in the solid domain. Even though the time step for each discretization is different, we observe a very good agreement between the three numerical solutions, with once again some discrepancies at the observation point located near the interface.

In Figure 4 we propose a graphic representation of the performances of the three different schemes. Comparing the reference with the simulation using ETC with a conform interface we observe an identical cost per iteration, as expected, but a significant improvement on the time step, also expected since the thin coating layer is not meshed. Finally, comparing the reference with the simulation using ETC with a non-conform interface we observe an important gain in both cost per iteration and time step, leading to an overall speedup of approximately $\times 15$ for a fixed global time window.

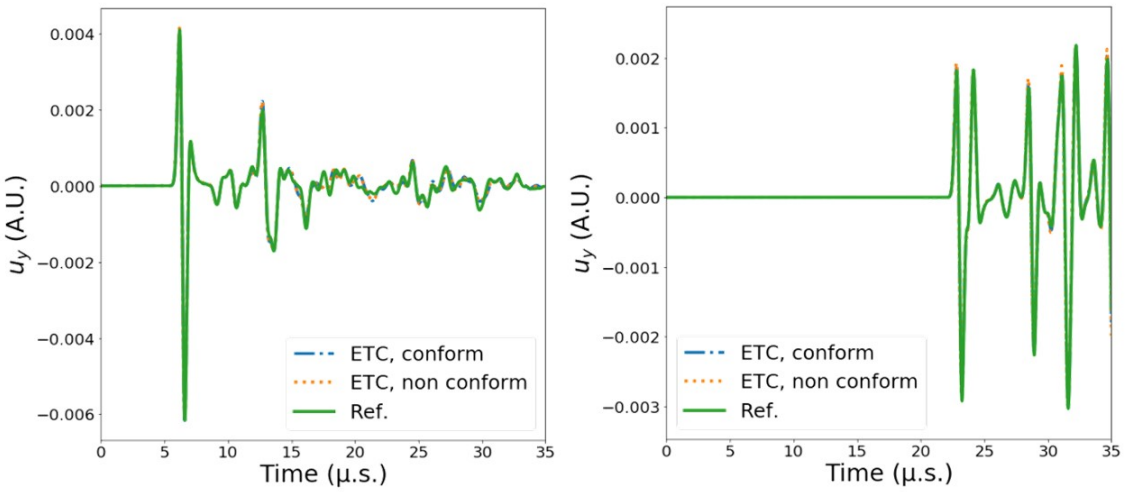

Figure 3: Comparing the time variation of the solution of the reference, ETC with conform interface and ETC with non-conform interface at the observation points P_0 (left) and P_1 (right).

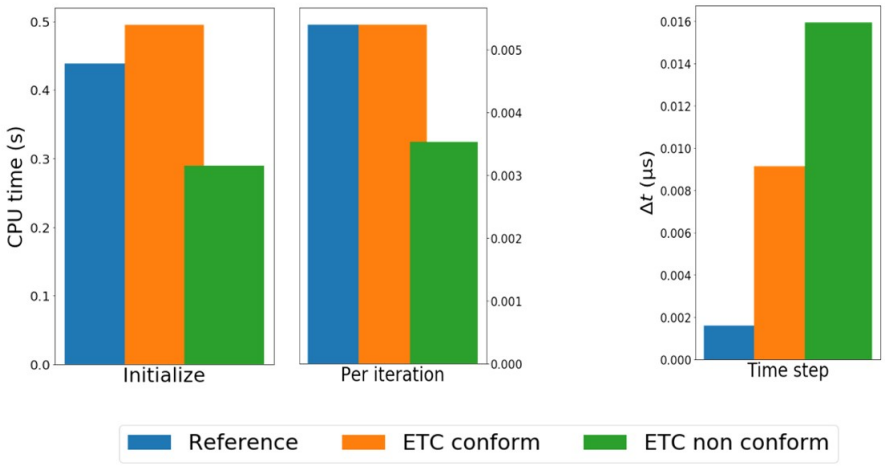

Figure 4: Comparing performances of the reference, ETC with conform interface and ETC with non-conform interface. The cost per iteration is divided by 1.52 and the time step is multiplied by 9.96, leading to an overall speedup of $\times 15$.

5 CONCLUSIONS AND PERSPECTIVES

In this communication we have presented a way to incorporate effective transmission conditions between a fluid wave propagator and a solid wave propagator using the mortar element method. This can typically be used to efficiently represent a thin layer between the fluid and solid domains. By using an implicit time scheme, the numerical illustrations suggest that the CFL condition of the presented numerical scheme becomes (compared to standard explicit discretization) independent of the thin layer thickness and the effective parameters. Additionnaly, relying on the flexibility of the mortar element method we are able to incorporate non-conform space discretizations between the fluid mesh and the solid mesh. Combining these two assets, we are able to obtain significant performance gains on relevant numerical simulations compared to a reference approach based on a standard fully explicit scheme with a meshed coating layer.

From a theoretical point of view, the natural perspective of this work is to be able to prove that the CFL condition is independent of the effective parameters. From a more numerical angle, we should investigate how the proposed numerical scheme performs on 3D cases or cases with curved interfaces.

REFERENCES

[1] Chabassier, J., and Imperiale, S. Fourth-order energy-preserving locally implicit time discretization for linear wave equations. *Int. J. Numer. Methods Eng.*, Vol. 106, no. 8, pp. 593–622, 2016.

[2] Ben Belgacem, F., and Y. Maday, The mortar element method for three dimensional finite elements. *ESAIM: M2AM* Vol. 31, no. 2, pp. 289–302, 1997.

[3] Diaz, J., and Grote, M. J., Energy conserving explicit local time stepping for second-order wave equations. *SIAM J. Sci. Comput.* Vol. 31, no. 3, pp. 1985–2014, 2009.

[4] Grote, M. J., Schneebeli A., and Schötzaun D. Discontinuous Galerkin finite element method for the wave equation. *SIAM J. Numer. Anal.* Vol. 44, no. 6, pp. 2408–2431, 2006.

[5] Rokhlin, S. I., and Y. J. Wang, Analysis of boundary conditions for elastic wave interaction with an interface between two solids. *J. Acoust. Soc. Am.* Vol. 29, no. 2, pp. 503–515, 1991.

[6] Bonnet, M., Burel, A., Duruflé, M., and Joly, P. Effective transmission conditions for thin-layer transmission problems in elastodynamics. The case of a planar layer model. *ESAIM: Math. Model. Numer. Anal.*, Vol. 50, no. 1, pp. 43–75, 2016.

[7] Imperiale, A., Leymarie, N., and Demaldent, E. Numerical modeling of wave propagation in anisotropic viscoelastic laminated materials in transient regime: Application to modeling ultrasonic testing of composite structures. *Int. J. Numer. Methods Eng.*, Vol. 121, no. 15, pp. 3300–3338, 2020.

[8] Joly, P. Variational methods for time-dependent wave propagation problems. *Topics in computational wave propagation. Springer, Berlin, Heidelberg*, pp.201-264, 2003

[9] Cohen, G. C. Higher-order numerical methods for transient wave equations. *Berlin: Springer, 2002* Vol. 5.

[10] Lombard, B., Piraux, J. How to incorporate the spring-mass conditions in finite difference schemes, *SIAM J. Sci. Comput.* Vol. 24, no. 4, pp. 1379 – 1407, 2003.

[11] Chabassier, J., and Imperiale, S. Stability and dispersion analysis of improved time discretization for simply supported prestressed Timoshenko systems. Application to the stiff piano string. *Wave Motion*, Vol. 50, no. 3, pp. 456–480, 2013.